Available online at www.sciencedirect.com
ScienceDirect
International Journal of Heat and Mass Transfer 50 (2007) 163–172
International Journal of HEAT and MASS TRANSFER
www.elsevier.com/locate/ijhmt

Microbubble return phenomena during subcooled boiling on small wires

Hao Wang [a,b], Xiaofeng Peng [a,*], Suresh V. Garimella [b], David M. Christopher [a]

[a] Laboratory of Phase-Change and Interfacial Transport Phenomena, Tsinghua University, Beijing 100084, China
[b] School of Mechanical Engineering, Purdue University, West Lafayette, IN 47907, USA

Received 1 November 2005; received in revised form 20 June 2006
Available online 24 August 2006

Abstract

An experimental investigation was conducted to explore the characteristics of subcooled boiling on microwires of 25 and 100 μm diameter. Microbubbles were observed to return to the wire surface after detachment, with two types of bubble return identified, i.e., isolated bubble return, and bubble return with liquid–vapor trailing jets. The former mode of bubble return occurred when isolated small bubbles (of less than 50 μm diameter) were generated from bubble collapse, while in the latter mode, a larger bubble (of up to 200 μm in diameter) at the end of a liquid–vapor jet issuing from the wire departed and then returned to the wire surface. The numerical simulations conducted show that the isolated bubble return is caused by large temperature gradients in the vicinity of the wire which lead to Marangoni flows and result in a strong thrust force driving the bubble back to the wire. Existence of large temperature gradients close to the microwire surface was demonstrated by experimental measurements, confirming numerical predictions. The numerical model accounts for the influence of noncondensable gas on the vapor saturation temperature as well as the interfacial condensation coefficient. The presence of noncondensable gas facilitates bubble return.

Keywords: Bubble dynamics; Bubble departure; Bubble return; Subcooled boiling; Microbubble; Microwire; Noncondensable gas

1. Introduction

The motion of bubbles near heated surfaces has significant consequences on boiling heat transfer and boiling regime transitions. Bubble departure, bubble coalescence, bubble motion along a heated surface, and the interactions among bubbles have been widely investigated [1–6]. With boiling finding newer applications in areas such as electronics cooling, bioengineering and spacecraft thermal control, there is need for a better understanding of bubble dynamics under the special conditions of these applications.

Detailed studies of bubble dynamics were undertaken by a number of researchers. Kowalewski and Pakleza [7] observed different kinds of bubble shapes at the moment of bubble departure. Depending on the heater size, surface superheat and the degree of liquid subcooling, the bubble shapes varied from spherical to strongly deformed columns of nearly cylindrical shape. For bubbles that were larger than 3 mm in diameter, the bottom surface was seen to be concave, with a conical hollow shape filling as much as half of the bubble. Shoji and Takagi [8] conducted a series of boiling experiments on artificially created nucleation sites with different geometries. Analysis of the time history of the wall temperature suggested the existence of low-dimensional chaos. Marek and Straub [20] studied the bubble behavior in subcooled pool boiling. A bubble in subcooled liquid could grow or shrink according to the heat and mass transfer at its top, and even a steady-state mass flow through the bubble could be maintained.

Greater diversity of bubble motion was visually observed under microgravity conditions. Small bubbles were observed to move towards larger bubbles, with the heat flux being increased by as much as 30% compared to similar experiments conducted under terrestrial conditions [9–11]. Straub [12] investigated boiling on a

* Corresponding author. Present address: Department of Thermal Engineering, Tsinghua University, Beijing 100084, China. Tel./fax: +86 10 62789751.
E-mail address: pxf-dte@mail.tsinghua.edu.cn (X. Peng).

0017-9310/$ - see front matter © 2006 Elsevier Ltd. All rights reserved.
doi:10.1016/j.ijheatmasstransfer.2006.04.038

Nomenclature

D_b	vapor bubble diameter (m)
D_w	heater wire diameter (m)
h_{fg}	latent heat of evaporation (J/kg)
h_i	equivalent interfacial heat transfer coefficient (W/m^2 K)
h_c	condensation coefficient (W/m^2 K)
h_e	evaporation coefficient (W/m^2 K)
$\overline{M}$	molecular weight (kg/mol)
$\overline{R}$	universal gas constant (J/mol K)
p_l	liquid pressure (N/m^2)
p_v	vapor pressure (N/m^2)
q''_w	wire surface heat flux (W/m^2)
q''_i	interfacial heat flux (W/m^2)
R	bubble radius (m)
T_b	liquid bulk temperature (K)
T_w	average wire temperature (K)
T_i	liquid temperature at interface (K)
T_s	saturation temperature (K)
T_v	vapor temperature (K)

Greek symbols

β	liquid thermal expansivity (1/K)
δ	liquid layer thickness (m)
θ	polar angle
ν	kinematic viscosity (m^2/s)
λ	thermal conductivity (W/m K)
μ	dynamic viscosity (Ns/m^2)
ρ_l	liquid density (kg/m^3)
ρ_v	vapor density (kg/m^3)
σ	surface tension coefficient (N/m)
$\hat{\sigma}$	accommodation coefficient

Subscripts

b	liquid bulk; bubble
c	condensation
e	evaporation
l	liquid
i	interface
s	saturated
v	vapor

0.26-mm-diameter spherical heater at a subcooling of 2–3 K. They observed that a bubble could stay suspended and immobile in the liquid a small distance away from the heated surface and then return to the surface, from which it departed again. Bubble coalescence was concluded to be one of the important factors for overall heat transfer and the evaporation of the micro liquid wedge between the bubble and the hot surface and the interfacial Marangoni flow were suggested as the dominant mechanisms for bubble motion under microgravity conditions [11,12].

For microbubbles, interfacial effects can generally be comparable to, or much greater than, gravitational effects. For example, a 100-μm-diameter water bubble has a buoyancy-to-surface tension ratio of order 10^{-4}. Under the strong influence of interfacial effects, microbubbles have been seen to exhibit interesting dynamic behaviors [15,16].

The present work investigates microbubble dynamics through boiling experiments conducted on very thin wires under terrestrial gravity conditions. Particular attention is paid to two types of bubble return phenomena. Visual observation of microbubbles produced in the experiments is complemented by theoretical analysis.

2. Experimental setup

The experimental apparatus used in the present study consisted of a test section, power supply and high-speed photography system, as schematically shown in Fig. 1(a). The test section is a transparent glass vessel with dimensions 23 cm × 23 cm × 23 cm in which a 49 mm long platinum wire of diameter 25 or 100 μm was installed in a

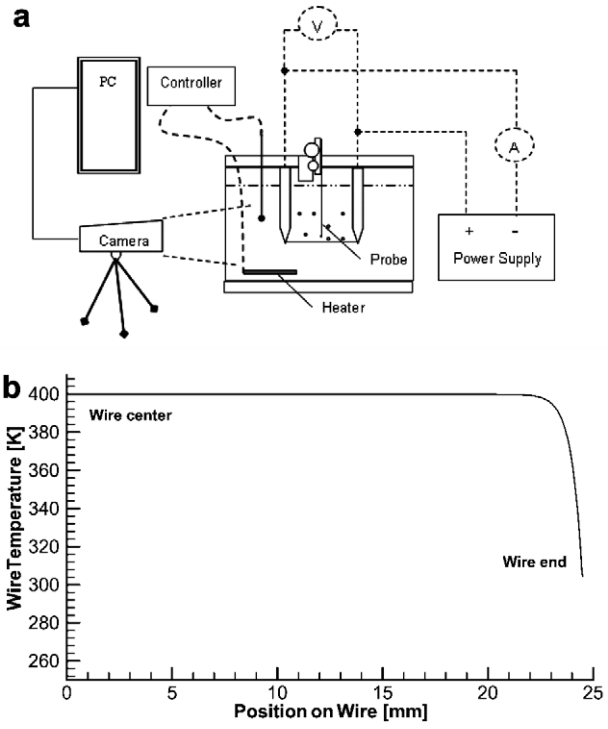

Fig. 1. (a) Experimental setup and (b) calculated temperature profile along the wire ($D_w = 100$ μm).

horizontal, vertical, or inclined orientation. The liquid level was 3–5 cm above the wire. The photographic system includes a high-speed CCD camera, a high-resolution image acquisition card, and zoom lenses. The Kodak SR-Ultra digital video camera (Motion Corder Analyzer SR series) has a capability of up to 10,000 frames per second at a resolution of 34 × 128 pixels. The sensor array of the camera is 658 × 496 pixels, with a pixel size of 7.4 μm × 7.4 μm. Recording rates of 500 fps, 1000 fps and 2000 fps were used in the experiments.

Deionized water (the effect of the presence of noncondensable gas in water is discussed later in this paper) and 95% alcohol at atmospheric pressure were used as the working fluids. A liquid subcooling level of greater than 30 K was always maintained.

The ends of the platinum wire were connected to a DC power supply through copper posts for heating. Both the current and voltage to the platinum wire were measured to determine the input power and wire resistance. The average wire temperature was determined using a calibrated correlation between the wire resistance and its temperature. The resistance of the wire was approximately a linear function of temperature, with the temperature coefficient found by calibration to be $3.85 \times 10^{-3}\ \mathrm{K}^{-1}$. Before each experimental run, the initial resistance of the wire was measured at the bulk temperature. The change in resistance was then recorded during the experiment and the corresponding temperature was deduced from the calibration curve. The uncertainty in wire temperature measurement is estimated to be ±3 K.

Heat loss from the ends of the wire by conduction to the copper posts was estimated to be less than 3% for the conditions of the experiments. Fig. 1(b) shows the computed temperature distribution in the wire at a uniform heat generation level of $3 \times 10^{10}\ \mathrm{W/m^3}$ and a heat transfer coefficient on the wire surface of $7500\ \mathrm{W/m^2K}$, for a bulk liquid temperature of 300 K. The heat lost from the ends is less than 2% of the total heat dissipation in this case.

A thermocouple probe mounted on a traverse was used to measure the temperature distribution in the vicinity of the wire. The thermocouple bead is approximately 100 μm in diameter, with the wire diameter being 37.5 μm. Another thermocouple located in the vessel more than 5 cm away from the wire was used to measure the bulk liquid temperature. A heater connected to a controller was immersed in the bulk liquid to set its temperature to the desired value.

Bubble locations and sizes were deduced by making measurements on the photographs obtained, after first calibrating the dimensions in the image to the physical dimensions of the experiment. Both bubble location and size are obtained to within an uncertainty of approximately 7%.

3. Bubble return phenomena

Two types of bubble return were visually identified, i.e., isolated bubble return, and bubble return with liquid–vapor trailing jets. These two bubble-return modes were observed only when the following conditions were satisfied: very small diameter wires (25 or 100 μm), bubbles at distances of less than 1 mm from the wire, and high degrees of subcooling (>30 K in the present work). The first mode of bubble return occurred when isolated small bubbles (less than 50 μm in diameter) were generated in water. This bubble return mode is shown through numerical analysis (Section 4) to be governed by Marangoni flow in the presence of steep temperature gradients near the wire surface. The second mode of bubble return was observed in alcohol with larger bubbles (of up to 200 μm diameter) at the end of a liquid–vapor jet issuing from specific nucleation sites. The bubble is seen to depart from the wire, stay briefly suspended at a small distance from the wire, and then return to the wire surface. Alternatively, the bubble forms and grows at the end of a liquid–vapor jet, and then returns to the wire surface.

3.1. Isolated bubble return

In the experiments with water at a relatively high heat flux ranging from 0.5×10^6 to $1.5 \times 10^6\ \mathrm{W/m^2}$, strong liquid jet flows with velocities of the order of 100 mm/s were observed to issue from the wire, as illustrated in Fig. 2. The burst velocity of the strong jets could be as high as 600 mm/s as estimated from video imaging; the jets propelled small bubbles, which were on the order of 10 μm in diameter, away from the wire into the bulk liquid.

It is speculated that this boiling mode consisting of strong jets and small bubbles is related to bubble collapse on the wire surface. It is seen in Fig. 2 that a bubble which

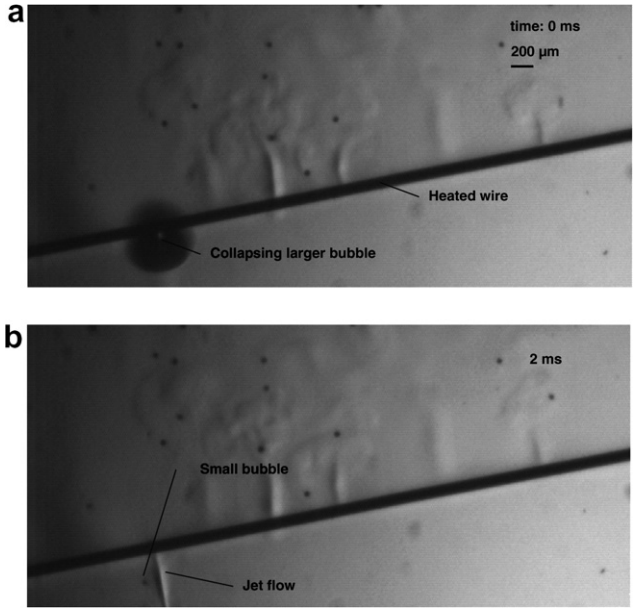

Fig. 2. Generation of a small bubble on the wire: (a) $t = 0$ s, a larger bubble is seen to collapse and (b) $t = 2$ ms, a tiny bubble and jet flow form subsequent to the collapse of the larger bubble (water, inclined wire $D_w = 100$ μm, $q''_w = 5.5 \times 10^5\ \mathrm{W/m^2}$, $T_w = 389$ K; $T_b = 353$ K, 500 fps).

is approximately 5–7 times the wire diameter collapses on the wire from Fig. 2(a) to (b) in 2 ms, followed by a jet flow ejecting a small bubble from the location where the larger bubble collapsed. Bubble collapse may be responsible for producing the high-speed jet flows observed, that is, the liquid rushes towards collapsing the bubble and then rebounded by the solid wall forming a jet flow which looks like issued from the wall.

Isolated bubble return often occurred when the jet flows was not intensive on the wire and small bubbles were able to linger in wire vicinity. During isolated bubble return, a single bubble returned to the wire and was not accompanied by other bubbles. A trajectory for a bubble return process is drawn in Fig. 3. It is seen bubble is bouncing on the wire. At 8, 16 and 26 ms the bubble returns and touches the wire surface. The largest return distance is about 200 μm. More often the return distance is about 50 μm (from 0 to 30 ms). During 8–12 ms and 40–60 ms the bubble is suspended above the wire.

From the curve for the bubble size it is seen that bubble was growing when closer to the wire which increased its buoyancy force and facilitated departing.

In Fig. 3, from 0 to 60 ms, there was no jet flow observed while after that several jet flows were observed successively erupting from the position below the bubble, as shown in Fig. 3(b). Bubble return phenomenon did not have to be with the jets. For example as in Fig. 5, the bubble departed and returned without any jet flow being observed. However, more detail work with aid of three-dimensional observations is highly needed to better understand the influence of the jets.

This mode of isolated bubble return was observed in the experiments for bubbles that were less than 50 μm in diameter and at a distance not greater than 300 μm from the wire surface.

A similar isolated bubble return phenomenon was also observed to occur on vertical wires, as shown in Fig. 4. A bubble is seen to move upward due to the buoyancy and the upward natural convection currents induced by the heated wire. However, the bubble repeatedly returns to the wire surface, in a "hopping" motion. On a horizontal wire (or one that is slightly inclined from the horizontal), some of the returning bubbles were observed to reattach to the wire and grow. With the wire being vertical, however, as in Fig. 4, the returning bubbles appear unable to reattach due to the strong upward flow along the wire. Weak shadows were noticed to mark the flow patterns around bubbles close to the wire during isolated bubble

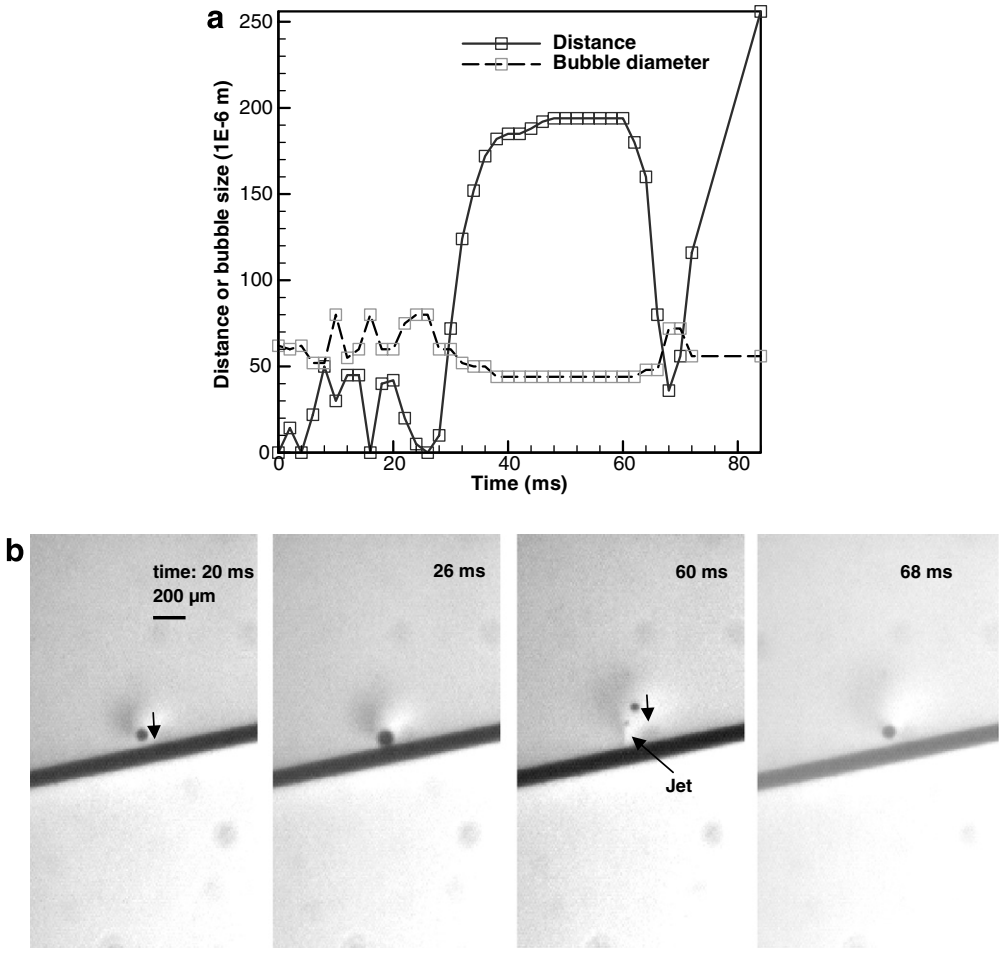

Fig. 3. Isolated bubble return (water, $D_w = 100$ μm, 500 fps, $q''_w = 7.0 \times 10^5$ W/m^2, $T_w = 379$ K, $T_b = 323$ K): (a) the evolution of bubble size and the distance from bubble bottom to wire; (b) corresponding frame images at different time points.

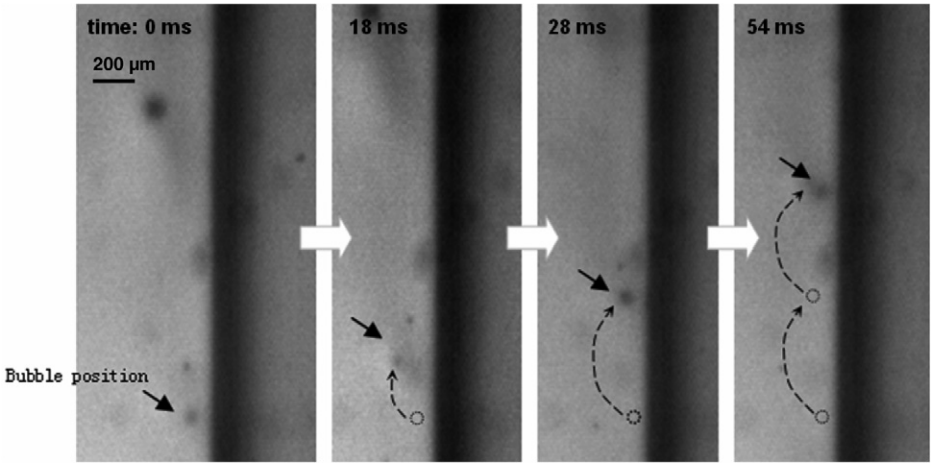

Fig. 4. Isolated bubble return phenomenon on a vertical wire (water, $D_w = 100$ μm, 500 fps, $q''_w = 5.5 \times 10^5$ W/m^2, $T_w = 377$ K, $T_b = 321$ K).

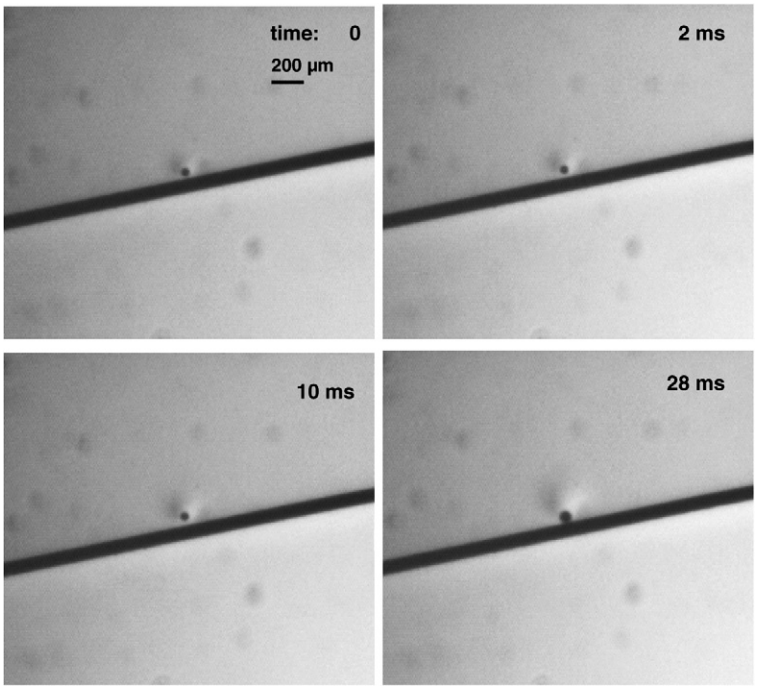

Fig. 5. A process of bubble return without jet flow influences (conditions as same as Fig. 3).

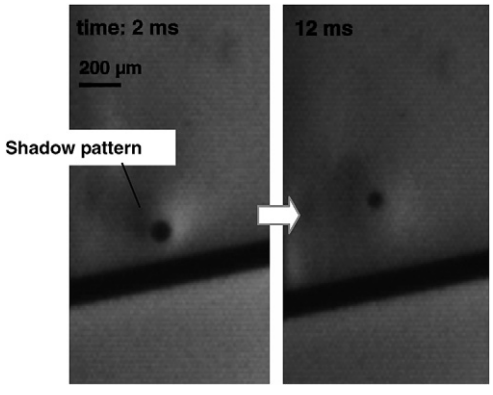

Fig. 6. Shadow pattern around an isolated small bubble (water, $D_w = 100$ μm, $q''_w = 5.3 \times 10^5$ W/m^2, $T_w = 376$ K, $T_b = 330$ K, 500 fps).

return, as captured with back-lighting in Fig. 6. The shadows were most visible with bubbles very close to the wire. As the bubble departed from the wire, the shadow became weaker, disappearing entirely once the bubble moved into the bulk liquid far from the wire. As discussed with the help of numerical predictions in the following, this shadow pattern highlights the temperature gradient around the bubble, which is an important driving force for bubble return.

3.2. Bubble return with liquid–vapor trailing jet

Unlike the return of small isolated bubbles observed in the experiments with water, a more complex bubble return phenomenon was observed in the experiments with alcohol. Wang et al. [17] observed liquid–vapor jet flows to issue

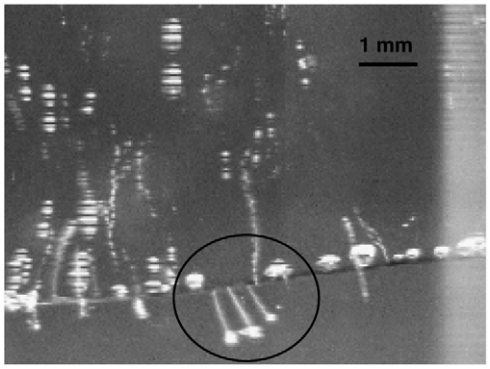

Fig. 7. Liquid–vapor jet flows issuing from nucleation sites [17].

from specific sites on a microwire in alcohol, a sample visualization of which is presented in Fig. 7. It was suggested [22] that these liquid–vapor jet flows issue from nucleation sites and are strongly governed by the complicated processes initiated within the nucleation sites. In the present work, these jets are seen to influence the second of the two modes of bubble return.

When a jet issuing from a nucleation site was topped by a bubble, then the vapor in the jet appears to feed the bubble, which increased in size and evolved into a larger bubble (larger than the jet diameter), as shown in Fig. 7. Fig. 8(a) shows two jets emanating from the wire. Large bubbles are clearly seen to have formed at the leading edge of the jets by $t = 6.8$ ms. These bubbles continued to grow in size and then returned towards the wire, almost reaching the wire at $t = 8.4$ ms.

Alternatively, Fig. 8(b) shows a bubble departing from the wire, followed by a liquid–vapor trailing jet ($t = 4$ ms) which is estimated to have an average velocity of approximately 15 mm/s. The jet appears to feed the bubble at its end; the balance between the vapor added by the jet at the bottom of the bubble and condensation of vapor on the other (top) end of the bubble lead to the maintenance of a relatively unchanged bubble size. After staying suspended at a small distance from the wire for a brief period, the bubble returned to the wire. At times the jet stopped issuing from the wire; when this happened, the bubble was observed to depart, not returning to the surface.

The phenomenon of bubble return accompanied by liquid–vapor trailing jets is remarkable in that the bubble appears to overcome forces exerted by the jet to push it away from the wire as well as the buoyancy force, and return to the wire. While a satisfactory explanation of this phenomenon cannot be offered at this time, the effects of Marangoni flow induced by the steep temperature gradients near the wire (discussed below with respect to isolated bubble return) no doubt play an important role in this second mode of bubble return as well.

4. Numerical analysis of isolated bubble return

As a first step towards developing physical explanations for the bubble return phenomena observed in the experiments, the isolated bubble return phenomenon is numerically investigated. It may be recalled that bubbles were found to return to the wire against the action of bubble

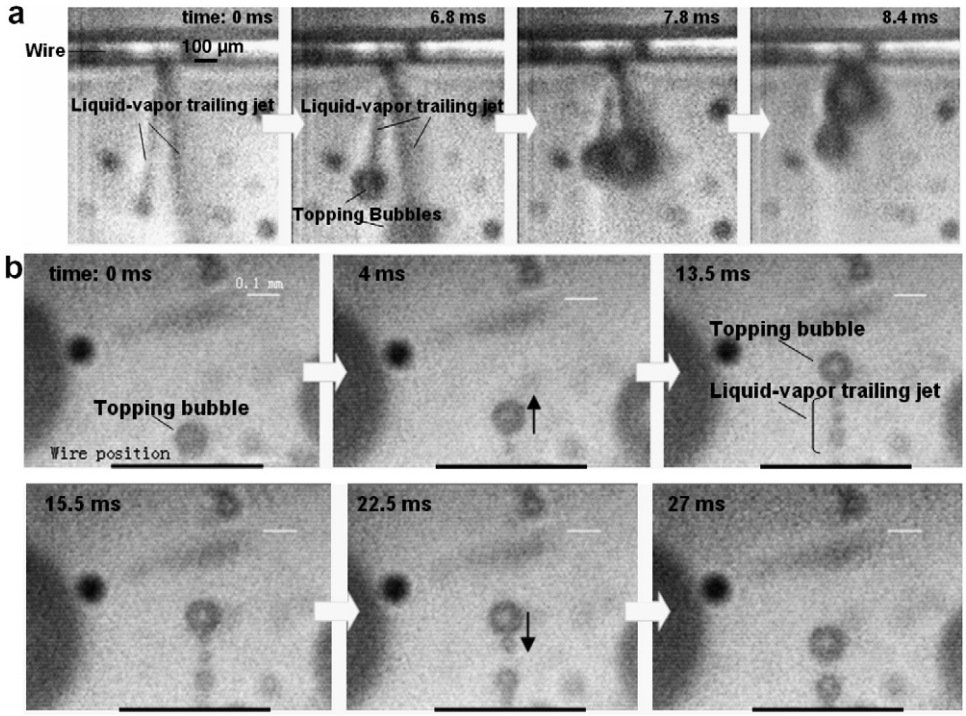

Fig. 8. Bubble return with liquid–vapor trailing jet: (a) larger bubble forms at the end of the jet issuing downwards, and returns to the wire (95% alcohol, $D_w = 100$ μm, $q''_w = 3.37 \times 10^5$ W/m^2, $T_w = 363$ K, $T_b = 311$ K, 500 fps); (b) larger bubble issues upward from the wire surface, trailed by a liquid–vapor jet, and also returns to the wire surface (95% alcohol, $D_w = 25$ μm, $q''_w = 1.7 \times 10^6$ W/m^2, $T_b = 314$ K; 2000 fps).

buoyancy and natural convection currents in the liquid due to the hot wire. To clarify the return mechanisms, therefore, the effects of bubble buoyancy, natural convection, interfacial phase-change heat transfer and Marangoni flow around the bubble were taken into account in the simulation. Due to the numerical difficulties with simulating a moving bubble, present work focuses on the state when the bubble suspended above the wire as during 8–12 ms and 40–60 ms in Fig. 3. The numerical model considers a bubble fixed at a distance of 100 μm (measured from the bottom of the bubble) above the wire surface, since the isolated bubbles were observed in the experiments to be suspended at roughly this distance after departure, before returning to the wire. The focus of the simulation is on the forces imposed on the bubble. If the net force on the bubble at this position is towards the wire, bubble return would be enabled.

4.1. Simulation domain

The simulation considers a single bubble suspended above a heated wire of diameter 100 μm and length 800 μm, as shown in Fig. 9. A three-dimensional, steady laminar model is developed to describe the fluid flow and associated heat transfer, with natural convection modeled using the Boussinesq approximation. A non-slip boundary condition is applied on the wire surface. The outer boundary of the computational domain is set as an open boundary with a specified bulk liquid temperature of 323 K and at atmospheric pressure. The diameter of the outer boundary is set as 2 mm, which is sufficiently large for boundary effects on the flow around the bubble to be negligible: The area-averaged velocity at the bubble surface was changed less than 1% when the diameter of the computational domain was increased to 5 mm. The wire temperature in the experiments was in the range of 377–390 K. In the simulation, the wire temperature was adjusted until the evaporation and condensation fluxes on the bubble were in equilibrium (since wire temperature influences the liquid temperature around the bubble); a wire temperature of 385.5 K resulted in the simulation, which agrees with the experimentally determined range.

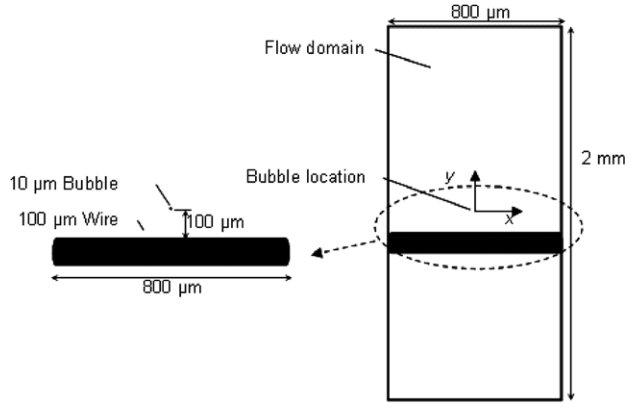

Fig. 9. The computational domain showing a 10-μm-diameter isolated bubble suspended 100 μm above the surface of the wire. (The flow domain included in the model is 2 mm in diameter by 0.8 mm in length. The bubble center is located at the origin $(x,y) = (0,0)$.)

The boundary conditions imposed at the bubble interface are critically important in this work. Treatment of condensation and evaporation heat transfer at the interface, as well as the Marangoni flow around the bubble induced by the interfacial tension gradient, is described below.

4.2. Phase-change heat transfer at bubble interface

Following a classical approach [13], the vapor temperature inside the bubble is obtained from the Laplace and Clausius–Clapeyron equations as

$$T_v = T_s + \frac{2\sigma T_s}{h_{fg}\rho_v R_b} \tag{1}$$

Assuming a uniform temperature T_v inside the bubble, the heat transfer occurring between the vapor and the interface is

$$q_i'' = h_i(T_v - T_i) \tag{2}$$

where h_i is the heat transfer coefficient between the interface and the vapor on the inside. For either evaporation or condensation, the heat transfer coefficient can be expressed as [18]

$$h_i = \frac{2\hat{\sigma}}{2-\hat{\sigma}}\frac{h_{fg}^2\rho_v}{T_v}\left(\frac{\overline{M}}{2\pi\bar{R}T_v}\right)^{1/2}\left[1-\frac{p_v}{2h_{fg}\rho_v}\right] \tag{3}$$

Paul [19] experimentally estimated the value of the accommodation coefficient, $\hat{\sigma}$, to be in the range of 0.02–0.04. In this investigation $\hat{\sigma}$ is taken as 0.03.

4.3. Estimation of the effects of noncondensable gas

In the experiments, it was noted that the bubbles did not shrink to zero diameter even when they moved into the subcooled bulk region, which suggests the existence of noncondensable gas inside the bubble. Noncondensables influence the saturation temperature T_v inside the bubble and heat transfer coefficients h_c and h_e between the interface and the vapor on the inside.

The partial pressure of gas P_{gas} can be estimated from Henry's law for a dilute solution, $P_{gas} = Hx$, in which x is the concentration of dissolved air in the bulk liquid. The value of x normally decreases as the liquid temperature increases. In the present experiments, the bulk liquid at the level of the returning bubble (100 μm from the wire) had a temperature in the range of 340–360 K, which corresponds to P_{gas} of 69% ~35% of the atmospheric pressure [21]. The partial pressure of vapor inside the bubble is estimated using Dalton's Law:

$$P_{vapor} = P_{bubble} - P_{gas}.$$

The vapor saturation temperature T_v can be evaluated from the vapor pressure P_{vapor}, and is found to be in the range of $355 \sim 365$ K. In the simulation, T_v is set to 360 K; higher values of T_v were also investigated in the simulation.

Besides its effect on the vapor temperature inside the bubble (via reduction of vapor partial pressure), the noncondensable gas in the bubble also influences the condensation coefficient. Marek and Straub [20] stated that the condensation heat transfer coefficient h_c could be reduced by as much as 90% if a small amount of noncondensable gas (such as a bulk mole fraction of 6%) exists in the vapor. By contrast, the evaporation coefficient h_e is not likely to be affected by the noncondensable gas because the gas tends to accumulate at the condensing portion of the surface inside the bubble. Since P_{gas} in the present work is estimated to be as high as 35–69% of atmospheric pressure, the condensation heat transfer coefficient h_c was approximated as having a value that is 1% of the evaporation coefficient h_e of 2.3×10^5 W/m^{2}K. The sensitivity of the simulation results to this choice was also examined by using higher values of condensation coefficient, as will be discussed in Section 5.3.

4.4. Marangoni effect

A temperature gradient exists along the bubble surface with the temperature increasing from the top to the bottom. The corresponding surface tension gradient induces Marangoni flow around the bubble. For steady interfacial flows, the balance of the interfacial shear forces under these conditions is given by

$$\tau_{R\theta} + \frac{1}{R}\frac{d\sigma}{dT}\frac{\partial T}{\partial \theta} + \tau'_{R\theta} = 0 \tag{4}$$

Since the vapor viscosity is usually very small, it is assumed that $\tau'_{R\theta} \approx 0$. Therefore, the interfacial boundary condition reduces to

$$\tau_{R\theta} = -\frac{1}{R}\frac{d\sigma}{dT}\left(\frac{\partial T}{\partial \theta}\right)_{r=R} \tag{5}$$

A value of -1.8×10^{-4} N/m K was used for the surface tension gradient with temperature for water [14].

4.5. Implementation

In view of the symmetry in the wire and bubble geometry, computations were performed over a quarter of the domain. The unstructured mesh for this quarter-domain contains 77,100 cells. Second-order upwind differencing was used for the advection terms, while the SIMPLE algorithm was employed for pressure–velocity coupling. The commercial software package, FLUENT 6, was used for the calculations. Four unstructured meshes of increasing coarseness, with 142,208, 92,310, 77,100, 36,038 cells, were tested to evaluate the mesh-independence of the results. The relative deviations in the computed drag force on the bubble relative to the finest mesh were 2.1%, 3.7% and 38.3%, respectively. The results obtained with the mesh with 77,100 cells were therefore considered sufficiently mesh-independent. The scaled convergence criteria imposed for continuity, momentum and energy equations were 1×10^{-5}, 1×10^{-5} and 1×10^{-8}, respectively.

5. Results and discussion

5.1. General characteristics

The predicted velocity field around the bubble with the Marangoni effect omitted (by setting $d\sigma/dT = 0$ in Eq. (5) and it is a non-shear boundary on the bubble surface) is shown in Fig. 10. It is seen the natural convection arising from the wire vicinity flows upward bypassing the bubble. The velocity on the bubble surface is caused by the bypassing flow, which is as low as 1 mm/s. With the Marangoni effect included, as in Fig. 11, liquid flow is observed from the bottom to the top of the bubble, and the highest velocity occurs at the bubble surface. The velocity contours in Fig. 11(b) provide a better delineation of the locations of maximum velocities.

The upward Marangoni flow on the bubble surface induces an opposing shear stress $\tau_{R\theta}$ per Eq. (5) which tends to push the bubble downward. (The liquid on the bubble surface is moving upward and the shear stress from the surrounding liquid is therefore downward; or by momentum conservation, when the bubble creates Marangoni flow flowing upward, the bubble will be thrust downward, analog to a plane propelling the air backward to make itself forward.) The total shear force in the y-direction on the bubble is computed to be -412.0×10^{-11} N (with the negative value implying that the force acts towards the wire), while the pressure force (hydrostatic and flow-induced) is 162.1×10^{-11} N. Thus the net force on the bubble is -249.9×10^{-11} N, acting towards the wire. This favors bubble return towards the wire.

If Marangoni effects were not included in the computation, no interfacial flow exists on the bubble (Fig. 10). Under this condition, the shear force on the bubble (due

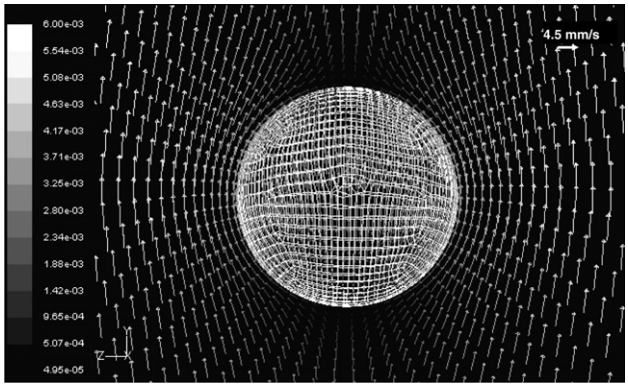

Fig. 10. Velocity field without Marangoni effects (the bubble is 100 μm above the heated wire, working fluid is water, $D_w = 100$ μm, $D_b = 10$ μm, $T_w = 385.6$ K, and $T_b = 323$ K).

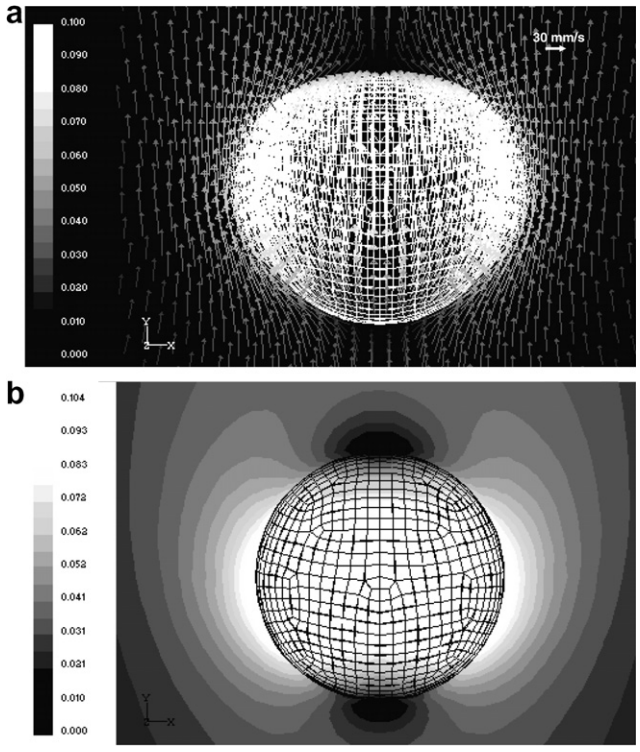

Fig. 11. Velocity field in the presence of Marangoni effects (the bubble is 100 μm above the heated wire, working fluid is water, $D_w = 100$ μm, $D_b = 10$ μm, $T_w = 385.6$ K, and $T_b = 323$ K): (a) velocity vectors (m/s) and (b) velocity contours (m/s).

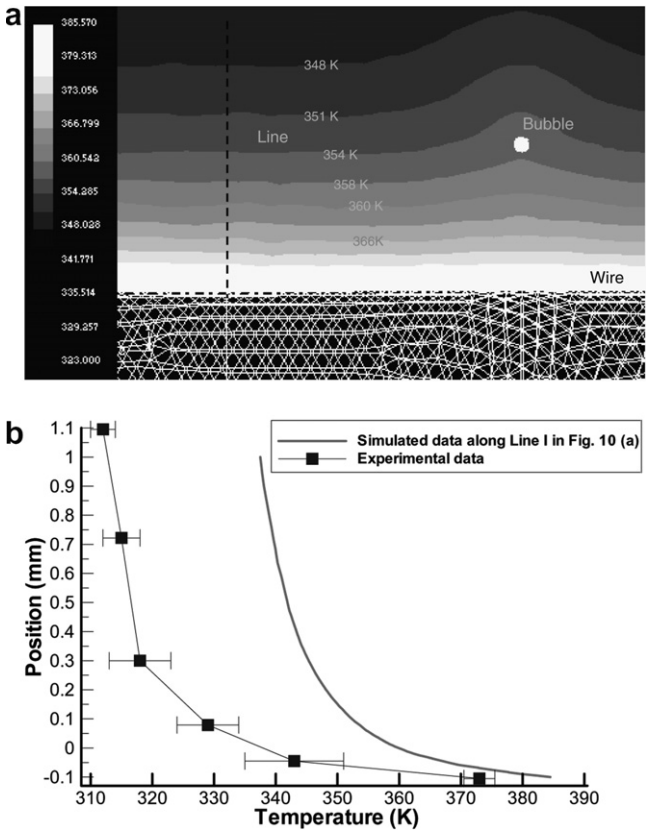

Fig. 12. Temperature field in the vicinity of the wire: (a) temperature contours above the wire and (b) temperature values along Line I (200 μm to the left of the bubble) in part (a), compared to thermocouple measurements, showing a sharp drop in temperature with distance from the wire. The upper surface of the wire in (b) is at −0.105 mm; wire and bulk temperatures in the simulation are 385.6 K and 323 K, respectively; wire and bulk temperatures in the experiment are 373 K and 301 K, respectively. The error bars on experimental symbols denote the temperature oscillations measured above the wire.

to upward natural convection from the wire) was 12.4×10^{-11} N while the pressure force was 5.6×10^{-11} N; since both forces are positive, the bubble would be lifted away from the wire. The simulation thus reveals the Marangoni effect to be the major driving mechanism for isolated bubble return.

5.2. Temperature field in vicinity of wire

It is clear from the results above that the temperature gradient near the heated wire plays a defining role in supporting the temperature gradient along the bubble surface (which is also influenced by the evaporation and condensation) which results in the observed Marangoni flow in Fig. 11. The temperature field in the vicinity of the wire and bubble in Fig. 12(a) shows that the temperature drops sharply with increasing distance from the wire surface. The temperature profile along Line I marked in Fig. 12(a) is shown in Fig. 12(b). This location is 200 μm to the left of the bubble, and the temperature field is not influenced by the presence of the bubble at this location, as revealed by the temperature contours being parallel to the wire surface. The temperature drops by 40 K over a distance of 300 μm from the wire. The existence of this steep temperature gradient near the wire was also demonstrated by experimental measurements in which a thermocouple (with bead diameter of ~100 μm) was used to measure the temperatures in the vicinity of the wire. The measurements in Fig. 12(b) show a comparable drop of approximately 50 K over the same distance, relative to the wire temperature (which was deduced from resistance–temperature calibration as explained previously).

5.3. Effect of noncondensable gas

The Marangoni effect is controlled by the temperature gradient along the bubble surface, which is in turn strongly influenced by the phase-change heat transfer at this surface. The results presented thus far were obtained under the assumption of an interfacial condensation coefficient which has a value of 1% of the evaporation coefficient of 2.3×10^5 W/m^2 K, to reflect the effect of noncondensable gases on the condensing surface in the bubble [20]. The temperature difference over the bubble surface was numerically computed to be 1.2 K under these conditions. If it is assumed that no noncondensable gas exists inside the bubble, such that the condensation and evaporation coefficients are equal, then the predicted temperature difference on the bubble surface reduces to 0.2 K. This

lower temperature difference results in a much weaker thrust on the bubble of -15.7×10^{-11} N, which is approximately one-sixteenth the thrust obtained in the presence of noncondensable gas. A higher condensation coefficient causes a more uniform surface temperature distribution on the bubble, leading to the weaker thrust force. The noncondensable gas inside the bubble thus decreases phase-change heat transfer and facilitates bubble return.

5.4. Effect of vapor temperature

The vapor temperature inside the bubble T_v was set to be 360 K in the results presented thus far, due to the assumed presence of noncondensable gas. In the absence of noncondensable gas, the saturation temperature of the vapor would be $T_v > 373$ K. If the saturation temperature is set to 373 K, the shear force on the bubble would be 592.0×10^{-11} N and the pressure force 240.8×10^{-11} N, leading to a thrust on the bubble of 241.2×10^{-11} N. This value is quite close to the result obtained in the presence of noncondensable gas (249.9×10^{-11} N), which indicates only a modest influence of the presence of noncondensables on the thrust experienced. However, the higher T_v increases the condensation heat flux from the vapor to the bubble surface, so that the wire temperature had to be increased to 407.1 K in this case to achieve equilibrium between the evaporation and condensation fluxes in the bubble. This high value of wire temperature is well above the temperatures in the experiments, indicating that noncondensable gas was indeed present in the experiments, with a corresponding suppression of T_v. Thus, while the vapor temperature does not significantly influence the thrust on the bubble directly, it does play an important role in bubble heat transfer.

6. Conclusions

An experimental and theoretical investigation was conducted to understand the dynamics of bubble generation, departure and return on microwires in a subcooled liquid. Two types of bubble return were observed in the experiments. The first, isolated bubble return, was observed for small bubbles with diameters less than 50 μm which were close to the wire. The second type of bubble return occurred when a bubble with a trailing liquid–vapor jet returned to the wire.

Large temperature gradients were found to exist close to the wire surface, both in the experiments and predictions. Numerical analysis for a 10 μm bubble that was 100 μm from the wire showed that Marangoni flow along the bubble surface from the bottom to the top produced the thrust that pushes the bubble back to the wire. Presence of noncondensable gas in the bubble increased the temperature gradient along the bubble surface and facilitated the bubble return process.

Acknowledgement

This research was supported by the Specialized Research Fund for the Doctoral Program of Higher Education (Contract No. 20040003076).

References

[1] L.E. Scriven, On the dynamics of phase growth, Chem. Eng. Sci. 10 (1959) 1–13.
[2] C.Y. Han, P. Griffith, The mechanism of heat transfer in nucleate pool boiling, Part I: Bubble initiation, growth and departure, Int. J. Heat Mass Transfer 8 (1965) 887–904.
[3] J. Straub, J. Winter, G. Picker, M. Zell, Study of vapor bubble growth in a supersaturated liquid, in: Proceedings of the National Heat Transfer Conference, Portland, Oregon, HTD-Vol. 305, ASME 3 (1995) 29–37.
[4] D.B.R. Kenning, Wall temperature patterns in nucleate boiling, Int. J. Heat Mass Transfer 35 (1992) 73–85.
[5] M. Shoji, T. Knhno, J. Negishi, et al., Chaos in boiling on a small size heater, in: Proceedings of fourth ASME-JSME Thermal Engineering Joint Conference, vol. 2, 1995, pp. 225–232.
[6] K. Cornwell, The role of sliding bubble in boiling on tube bundlesHeat Transfer 1990 (9th International Heat Transfer Conference, Jerusalem), Hemisphere, New York, 1990, pp. 455–460.
[7] T.A. Kowalewski, J. Pakleza, Visualization of vapor bubble growth, in: 9th International Symposium on Flow Visualization, 2000, No. 176.
[8] M. Shoji, Y. Takagi, Bubbling features from a single artificial cavity, Int. J. Heat Mass Transfer 44 (2001) 2763–2776.
[9] H.S. Lee, H. Merte, F.P. Chiaramonte, Pool boiling phenomena in microgravity, in: Proceeding of 11th International Heat Transfer Conference, Korea, Taylor and Francis, vol. 2, pp. 395–400.
[10] M. Zell, J. Straub, B. Vogel, Pool boiling under microgravity, J. Phys.–Chem. Hydrodyn. 11 (1989) 813–823.
[11] J. Straub, The role of surface tension for two-phase heat and mass transfer in the absence of gravity, Exp. Therm. Fluid Sci. 9 (1994) 213–233.
[12] J. Straub, Microscale boiling heat transfer under 0*g* and 1*g* conditions, Int. J. Therm. Sci. 39 (2000) 490–497.
[13] M.H. Shi, Y.P. Gan, C.F. Ma, Boiling Heat Transfer and Condensation, Higher Education Press, Beijing, 1995.
[14] X.C. Fu, W.X. Shen, T.Y. Yao, Physics and Chemistry, Higher Education Press, Beijing, 1990.
[15] H. Wang, X.F. Peng, W.K. Lin, C. Pan, B.X. Wang, Bubble-top jet flow on micro wires, Int. J. Heat Mass Transfer 47 (2004) 2891–2900.
[16] H. Wang, X.F. Peng, B.X. Wang, D.J. Lee, Bubble-sweeping mechanisms, Sci. China, Ser. E 46 (2003) 225–233.
[17] H. Wang, X.F. Peng, B.X. Wang, D.J. Lee, Jet flow phenomena during nucleate boiling, Int. J. Heat Mass Transfer 45 (2002) 1359–1363.
[18] V.P. Carey, Liquid–vapor phase-change phenomena, Hemisphere, New York, 1992, pp. 112–120.
[19] B. Paul, Complication of evaporation coefficients, ARS J. 32 (1962) 1321–1328.
[20] R. Marek, J. Straub, The origin of thermocapillary convection in subcooled nucleate pool boiling, Int. J. Heat Mass Transfer 44 (2001) 619–632.
[21] S. Petrovic, T. Robinson, R.L. Judd, Marangoni heat transfer in subcooled nucleate pool boiling, Int. J. Heat Mass Transfer 47 (2004) 5115–5128.
[22] H. Wang, Multiplicity of nucleation and near-wall bubble dynamics of subcooled boiling on micro wires, Ph.D. Thesis, Tsinghua University, Beijing, 2004.